The effect of the positron distribution and electron–positron correlations on the electron–positron momentum density for SiC

2008 J. Phys.: Condens. Matter 20 335226

(http://iopscience.iop.org/0953-8984/20/33/335226)

J. Phys.: Condens. Matter **20** (2008) 335226 (10pp) doi:10.1088/0953-8984/20/33/335226

The effect of the positron distribution and electron–positron correlations on the electron–positron momentum density for SiC

Anna Rubaszek

W Trzebiatowski Institute of Low Temperatures and Structure Research, Polish Academy of Sciences, 50-950 Wroclaw 2, PO Box 1410, Poland

E-mail: A.Rubaszek@int.pan.wroc.pl

Received 14 February 2008, in final form 11 July 2008
Published 31 July 2008
Online at stacks.iop.org/JPhysCM/20/335226

Abstract

To interpret the data on positron annihilation in solids in terms of the electron momentum density, both the electron–positron interaction and the positron distribution have to be considered explicitly. In this work we discuss the influence of the shape of the positron wavefunction and electron–positron (e–p) correlations on the calculated e–p momentum density and lifetime of the positron in perfect SiC. It is shown that the form of the positron distribution in the Wigner–Seitz cell has a considerable effect on the calculated annihilation characteristics. The results obtained within the independent particle model are compared with their counterparts incorporating e–p correlation functions locally and beyond the local density approximation. The calculations have been performed for SiC of 3C cubic (zinc-blende) structure within the linear muffin-tin orbital atomic sphere approximation method.

1. Introduction

Positron annihilation spectroscopy is a sensitive and effective technique to probe the electronic structure of solids [1]. In particular, the angular correlation of annihilation radiation (ACAR) and coincidence Doppler broadening experimental data contain useful information on the electron momentum density (EMD) in the material under study.

The increasing interest in the electronic properties of silicon carbide [2, 3] is mainly due to the vital importance of this semiconductor for industry and device technology. The positron annihilation characteristics for perfect and defected SiC have been extensively studied both theoretically and experimentally [4–8]. However, due to strong Coulomb attraction between the positron and surrounding electron cloud, the information on the electron density in SiC, extracted from the ACAR [4, 5] and Doppler broadening spectra [4] as well as from the positron lifetime [6, 7], is distorted by the effect of both the positron distribution and enhancement of electron density at the positron site. While the resulting change of the electron density at the positron position has been widely studied (see [1, 9–13] and references cited therein), much less attention has been given to the influence of the positron distribution on the calculated annihilation characteristics in solids [9, 10].

In the present paper the effect of the positron wavefunction on the calculated e–p momentum density is studied for the perfect SiC of the 3C zinc-blende structure. Moreover, the influence of the e–p interaction on the positron charge distribution is discussed. The annihilation characteristics obtained within the local and non-local approaches to the e–p correlation are compared with their independent particle model (IPM) and EMD counterparts. The valence and core contributions to the resulting spectra are analysed thoroughly.

2. Calculation and results

The experimental ACAR and Doppler broadening spectra are usually interpreted as, respectively, two- and one-dimensional projections of the e–p momentum density. This density is given by the formula:

$$\rho(\mathbf{p}=\mathbf{k}+\mathbf{G}) = \sum_t \left| \int_\Omega \exp(-\mathrm{i}\mathbf{p}\cdot\mathbf{r})\psi_t(\mathbf{r})\psi_+(\mathbf{r})\sqrt{\gamma(t,\mathbf{r})}\,\mathrm{d}\mathbf{r} \right|^2. \quad (1)$$

Here **p** and **k** are the momenta in the extended and reduced zone scheme, respectively, **G** is the reciprocal lattice vector and Ω is the volume of the sample. ψ_+ and ψ_t stand for the positron and electron wavefunctions, respectively, and γ denotes the e–p correlation function that, in general, depends on both the initial electron state t and the positron position **r**. The summation in equation (1) runs over all occupied electron states t, which for valence electrons are the Bloch states $\mathbf{k}j$ (associated with the wavevector **k** and band index j), and for core sates are indexed by quantum numbers nlj.

Within the IPM the e–p correlation effect is neglected, i.e. one assumes that $\gamma(t, \mathbf{r}) = 1$, and formula (1) takes the form:

$$\rho^{\mathrm{IPM}}(\mathbf{p} = \mathbf{k} + \mathbf{G}) = \sum_t \left| \int_\Omega \exp(-\mathrm{i}\mathbf{p}\cdot\mathbf{r})\psi_t(\mathbf{r})\psi_+(\mathbf{r})\,\mathrm{d}\mathbf{r} \right|^2. \tag{2}$$

If the positron is uniformly distributed in the unit cell, i.e. if one assumes that $|\psi_+(\mathbf{r})|^2 = 1/\Omega$, then the IPM formula (2) reduces to the expression which defines the EMD:

$$\rho^{\mathrm{EMD}}(\mathbf{p} = \mathbf{k} + \mathbf{G}) = \sum_t \left| 1/\sqrt{\Omega} \int_\Omega \exp(-\mathrm{i}\mathbf{p}\cdot\mathbf{r})\psi_t(\mathbf{r})\,\mathrm{d}\mathbf{r} \right|^2. \tag{3}$$

The electron and positron wavefunctions in formulae (1)–(3) are the solutions of the set of Schrödinger equations,

$$[-\nabla^2 + V_{\mathrm{ext}}(\mathbf{r}) + V_{\mathrm{H}}(\mathbf{r}) + V_{\mathrm{xc}}(\mathbf{r})]\psi_t(\mathbf{r}) = E_t\psi_t(\mathbf{r}) \tag{4a}$$

$$[-\nabla^2 - V_{\mathrm{ext}}(\mathbf{r}) - V_{\mathrm{H}}(\mathbf{r}) + V_{\mathrm{corr}}(\mathbf{r})]\psi_+(\mathbf{r}) = E_+\psi_+(\mathbf{r}). \tag{4b}$$

The electron Coulomb potential, V_{C}, consists of the Hartree potential and the external potential, due to ions, V_{H}, and V_{ext}. The relevant positron Coulomb potential is equal to its electron counterpart with the opposite sign. V_{corr} and V_{xc} denote the e–p interaction [1, 11] and e–e exchange–correlation potentials, respectively. The electron charge density,

$$n_{\mathrm{el}}(\mathbf{r}) = \sum_t |\psi_t(\mathbf{r})|^2,$$

and the Hartree potential are related as

$$V_{\mathrm{H}}(\mathbf{r}) = \int_\Omega n_{\mathrm{el}}(\mathbf{r}')/|\mathbf{r} - \mathbf{r}'|\,\mathrm{d}\mathbf{r}'.$$

The potential V_{corr} describes the positron interaction with the electron screening cloud and can be determined from the Feynman theorem [1, 10, 11], basing on the screening charge distribution. Although several approximations, local or non-local, exist for the e–p interaction, in most theoretical studies of the positron annihilation characteristics the correlation potential V_{corr} has been set equal to zero. The latter approach is due to the IPM [1]. Local density approximation (LDA) [9, 11] to the density functional theory approximates this e–p potential by a local quantity corresponding to the homogeneous electron gas, and therefore is not expected to work well for strongly varying electron densities. For the latter, the non-local effects will be important and they can be described, for example, within the generalized gradient approximation (GGA) [12] or the weighted density approximation (WDA) [10, 14].

In the present work the valence electron and positron wavefunctions have been calculated for SiC of 3C cubic (zinc-blende) structure using the self-consistent linear muffin-tin orbital (LMTO) band structure scheme with the atomic sphere approximation (ASA) [15, 16]. For the core electrons the relativistic effects are included. The experimental lattice constant, $a = 8.22$ au [2], has been used. The 3C cubic zinc-blende structure of SiC has been modelled within the ASA as the fcc lattice containing four spheres in the unit cell. Two of the spheres are centred at $\boldsymbol{q}_1 = (0, 0, 0)$ on the Si site and at $\boldsymbol{q}_2 = (a/4, a/4, a/4)$ on the C site. To improve the packing of the open zinc-blende structure, the two empty spheres have been included. These spheres, positioned at $\boldsymbol{q}_3 = (a/2, 0, 0)$ and $\boldsymbol{q}_4 = (3a/4, a/4, a/4)$, represent the interstitial region. The relevant value of the average sphere radius, S, equals to 2.024 au. In the present calculation the radii of individual atomic spheres have been set equal to the common average value, S. To improve on the ASA, for valence part of $\rho(\boldsymbol{p})$ the Jarlborg–Singh correction [17] has been implemented in the equations (1)–(3).

The electron–electron exchange–correlation potential has been incorporated in (4*a*) within the LDA in the Ceperley–Alder form [18]. The GGA [19] was also employed for comparison. The positron wavefunction has been associated with the bottom of positron energy band ($\boldsymbol{k}_+ = \mathbf{0}$, $j_+ = 1$). Various approximations to V_{corr} have been applied in the positron Schrödinger equation. The e–p momentum density has been calculated for the IPM and including the e–p interaction effects within the LDA and WDA.

2.1. The electronic structure

The electron Coulomb potential in the sphere of type q takes the form

$$V_{\mathrm{C}}^q(r) = V_{\mathrm{H}}^q(r) + V_{\mathrm{ext}}^q(r) = \int_{\Omega_q} n_{\mathrm{el}}^q(\mathbf{r}')/|\mathbf{r} - \mathbf{r}'|\,\mathrm{d}\mathbf{r}' - Z^q/r + V_{\mathrm{mad}}^q,$$

where Z^q and n_{el}^q denote the nucleus charge and electron density distribution in the sphere. $SV_{\mathrm{H}}^q(S)$ is equal to the electron charge inside the sphere of volume Ω_q and V_{mad}^q is the respective Madelung potential. For the sphere positioned at $\boldsymbol{q}$, V_{mad}^q is defined as [15, 16]

$$V_{\mathrm{mad}}^q = -1/S \sum_{\mathbf{R},\mathbf{q}'} \Delta Z^{q'}/|\mathbf{R} - \mathbf{q} + \mathbf{q}'|,$$

where **R** are the lattice vectors and $\Delta Z^q = Z^q - SV_{\mathrm{H}}^q(S)$ is the charge (ionicity) of the sphere q.

The calculated valence electron band structure along three main crystallographic directions is shown in figure 1. Solid and broken lines correspond, respectively, to the LDA [18] and GGA [19] electron–electron exchange–correlation potential, V_{xc}, employed in (4*a*). Eight valence electrons fully occupy four lower bands. Due to the charge neutrality of the unit cell in SiC, the sum of Coulomb potentials at the sphere boundaries is equal to zero,

$$\sum_q V_{\mathrm{C}}^q(S) = 0,$$

and well defines the zero energy level.

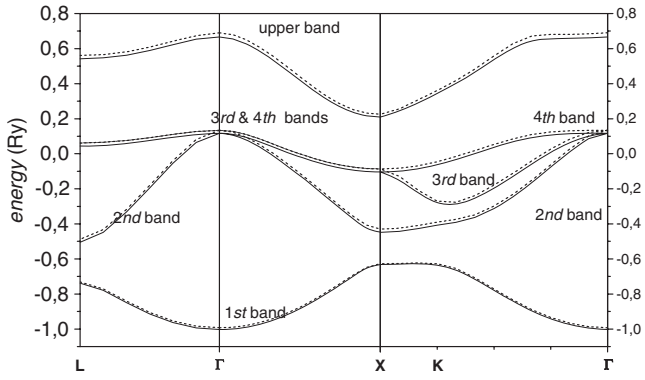

Figure 1. Energy bands in SiC along three main crystallographic directions. Solid and broken lines correspond to the LDA [18] and GGA [19] to V_{xc}, respectively.

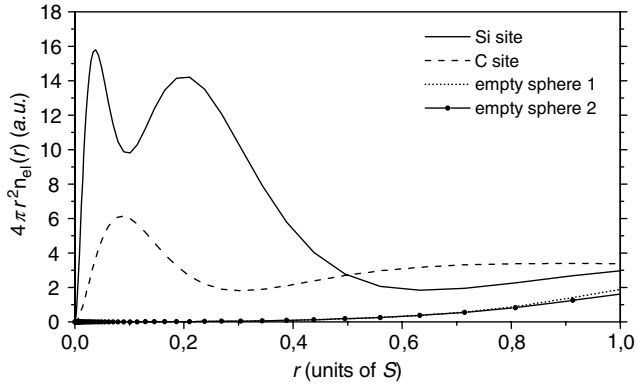

Figure 2. Electron charge density inside individual atomic spheres calculated as a function of the distance from the centre for the spheres containing atoms of Si and C and for the empty spheres.

Table 1. The positron and valence electrons charge contained inside the individual atomic spheres, calculated within various approaches to the e–p and e–e interaction potentials.

	Positron charge				Valence electrons charge	
Sphere	IPM	LDA	WDA	$1/\Omega$	LDA	GGA
Si site	0.104	0.112	0.118	0.25	1.985	1.964
C site	0.148	0.164	0.179	0.25	4.328	4.348
Empty sphere 1	0.418	0.405	0.395	0.25	0.877	0.875
Empty sphere 2	0.330	0.319	0.308	0.25	0.812	0.813

As can be seen in figure 1, the results for the LDA and GGA energy band structures hardly differ. The calculated electron chemical potentials, μ_-, that contribute to the positron affinity [6, 20], are equal to 0.117 and 0.134 Ryd for the LDA and GGA, respectively. The relevant values of energy gap, E_{gap}, equal to 2.16 and 2.14 eV, are slightly lower than the reported experimental data, 2.36 eV [2].

The radial distribution of the electron charge inside the individual spheres, $4\pi r^2 n_{el}^q(r)$, obtained within the LDA, is plotted in figure 2. The valence electron charge is polarized in the Wigner–Seitz cell [3]. In contrast to the unit cell, the separate atomic spheres are not neutral any more. The electron charge transfers from the Si site towards the C site and the two empty spheres. The ionicity ΔZ^q of the sphere positioned at the Si atom ($Z = 14$), calculated within the LDA and GGA amounts to 2.017 and 2.036, respectively. The relevant LDA and GGA values for the sphere at the C site ($Z = 6$) are equal to -0.328 and -0.348. For the two empty spheres ($Z = 0$), centred at $\boldsymbol{q}_3$ and $\boldsymbol{q}_4$, the corresponding charges are equal to -0.877 and -0.812 for the LDA and to -0.875 and -0.813 for the GGA. The charge of valence electrons in particular spheres is listed in table 1. The major part of valence charge (about 55%) is contained inside the sphere positioned at the C atom and at the Si site (about 25%). The remaining valence charge (about 20%) is distributed almost equally between the two empty spheres.

The lack of charge neutrality for individual spheres gives rise to non-zero values of the Coulomb potential at the spheres boundary, $V_C^q(S)$ (the slope of $-r^2 V_C^q(r)$ is presented in figure 3 by solid lines). In consequence, the corresponding electron densities, $n_{el}^q(S)$, differ for various spheres, as can be well seen in figure 2.

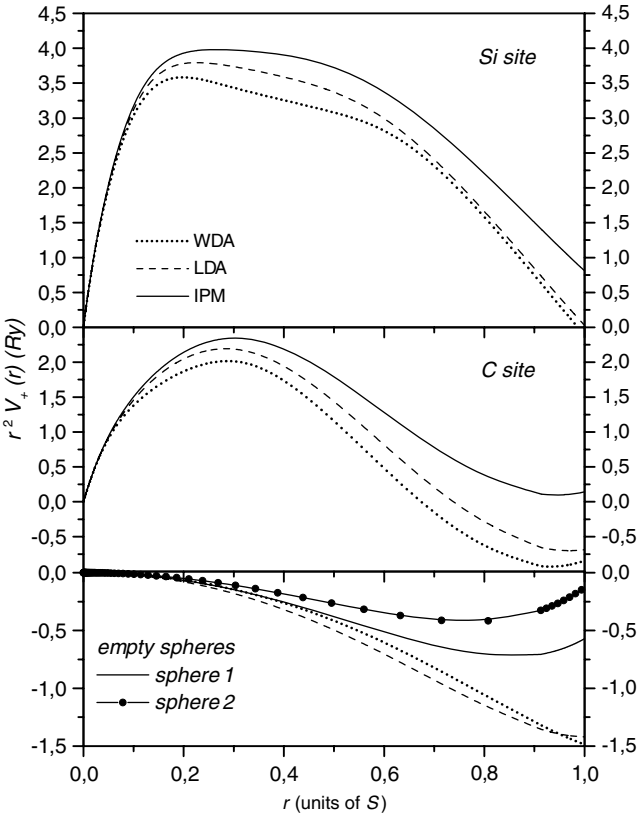

Figure 3. The positron potential, $r^2 V_+(r)$, inside the individual spheres as a function of the distance r from the sphere centre, calculated within the IPM, LDA and WDA to V_{corr}. Circles mark the IPM for the empty sphere centred at $\boldsymbol{q}_4$.

2.2. The positron distribution

The effective potential, acting on the positron (see (4*b*)), is presented in figure 3 for individual spheres. The IPM result corresponds to neglecting the e–p interaction, i.e. to

$V_{\rm corr}(r) = 0$, and is equal to the electron Coulomb potential with the opposite sign. This quantity is plotted for the spheres positioned at $\boldsymbol{q}_1$ (Si site), $\boldsymbol{q}_2$ (C site) and $\boldsymbol{q}_3$ (empty sphere) by solid lines. Solid circles describe second empty sphere, centred at $\boldsymbol{q}_4$.

The e–p correlation effects have been incorporated in (4*b*) both locally and beyond the LDA. The LDA results, as parameterized by Boronski and Nieminen [11], are presented by dashed lines for the spheres centred at $\boldsymbol{q}_1$, $\boldsymbol{q}_2$ and $\boldsymbol{q}_3$. The non-locality of $V_{\rm corr}$ has been implemented within the WDA [10] (the dotted lines in figure 3). The energy dependent correlation functions have been used in the calculation of $V_{\rm corr}^{\rm WDA}$ from the Feynman theorem. The semiconductor character of SiC is taken into account by including the non-zero value of the energy gap to the state-selective WDA formalism. For the sake of fitting to the graph scale, the plots of LDA and WDA potentials refer to $V_+^{\rm LDA}(r) + 0.5$ Ryd and $V_+^{\rm WDA}(r) + 0.5$ Ryd, i.e. to the positron potential shifted by a constant value of 0.5 Ryd (equal to the positron binding energy).

The first thing to note when comparing the curves in figure 3, is that the IPM result differs appreciably from its LDA and WDA counterparts, as the 'bare' positron is more repulsive to ionic cores than the particle 'dressed' in its screening cloud. Inside the Si and C spheres, the LDA values are intermediate between the IPM and WDA. This feature may be attributed to the fact, that the electron screening cloud, evaluated within the WDA, is shifted from the positron position towards the region, where the electrons are found with highest probability [10]. In the empty sphere the WDA screening charge is partially detached from a positron and redistributed towards the 'full' spheres. In consequence, the WDA potential is more IPM-like than its LDA counterpart. Close to the boundary of the sphere positioned at the Si site and in the empty sphere, the LDA and WDA potentials are more similar, as in this region the electron density varies rather slowly (as can be seen in figure 2). This is not the case for the positron position close to the nuclei, where the electron density is varying stronger and the non-locality of the e–p correlations starts to play an important role.

The positron energy eigenvalues, E_+, obtained from (4*b*) within the IPM, LDA and WDA, amount to 0.115, −0.513 and −0.519 Ryd, respectively. The common zero energy level has been set for the positron and electrons. The positron affinity, A_+, has been introduced for a bulk material as the sum of electron and positron chemical potentials [6, 20]. For the LDA [18] electron model in (4*a*), the relevant values of A_+ are equal to 0.32, −5.39 and −5.96 eV for the IPM, LDA and WDA positron potentials in (4*b*), respectively. The application of the GGA [19] to the e–e exchange–correlation potential in (4*a*) changes relevant values only slightly, to −5.15 and −5.24 eV for the LDA and WDA positron potentials. In both cases the theoretical results differ from the value of −3.89 eV [6], extracted from the experimental data as the sum of measured electron and positron work functions. On the other hand, the values of A_+, calculated in the present work, are in a very good agreement with the theoretical results of [6].

The positron density distribution in the individual spheres, $|\psi_+(r)|^2$, calculated within various approaches to $V_{\rm corr}$ in (4*b*), is presented in figure 4 as a function of the distance r from the sphere centre. Once again, the curves marked by the solid circles refer to the second empty sphere, located at $\boldsymbol{q}_4$. The dash-dotted line corresponds to the uniform positron distribution. The relevant positron charge, contained in the separate spheres, is listed in table 1 for the IPM, LDA and WDA approximation to $V_{\rm corr}$.

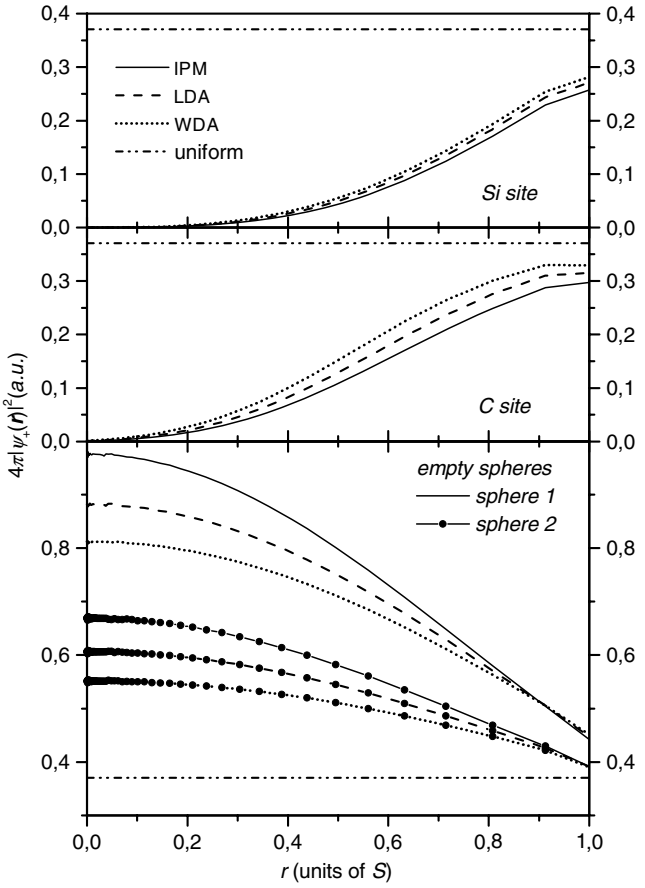

Figure 4. The positron density distribution calculated within various approximations, as a function of distance from the centre of the spheres containing Si and C atoms (two upper panels) and of the two empty spheres (bottom panel). IPM, LDA and WDA refer to the approach used for $V_{\rm corr}$ in (4*b*). The uniform distribution, $|\psi_+(r)|^2 = 1/\Omega$, is quoted by the dash-dotted lines.

As can be seen in figure 4 and table 1, the positron distribution has the highest weight (over 70%) just in the interstitial region, represented by the empty spheres. There is a strong influence of the e–p interaction on the shape of the positron wavefunction, through the e–p correlation potential. Comparing the results obtained within the IPM, LDA and WDA, one can note that the inclusion of the e–p correlation potential in (4*b*) shifts the positron weight from the empty spheres towards the C and Si site. This effect, observed for both the LDA and WDA approaches, is easy to understand since the 'dressed' positron is more neutral to ions. The non-locality of the e–p interaction, taken into account within the WDA, enhances the above redistribution of the positron charge in the Wigner–Seitz cell as compared to the LDA approach. The explanation is that the positron is mainly screened by the valence electrons, which are found with the highest probability

at the C and Si site (as shown in table1). Within the WDA, the positron follows its screening cloud towards the C and Si atoms.

2.3. Electron–positron momentum density and positron lifetime

The experimental positron lifetime, τ, is a unique characteristic of the material. This quantity is calculated as inverse of the total annihilation rate, $\lambda = 1/\tau$, which is related to $\rho(\boldsymbol{p})$ directly, according to the formula

$$\lambda = \pi r_0^2 c\Omega/(2\pi)^3 \int \rho(\mathbf{p})\,\mathrm{d}\mathbf{p}$$
$$= \pi r_0^2 c \sum_t \int_\Omega n_{\mathrm{el}}^t(\mathbf{r})|\psi_+(\mathbf{r})\sqrt{\gamma(t,\mathbf{r})}|^2\,\mathrm{d}\mathbf{r}, \qquad (5)$$

where r_0 and c denote the classical electron radius and velocity of light, respectively. Index t in (5) stands for the type of electrons, core and valence. For valence electron density the shell separation [15, 16] has been implemented and type t is associated with the angular momentum, l. It is apparent from (5) that all the effects observed in the e–p momentum density are expected to reproduce in the relevant core and valence components of the total annihilation rate.

In this subsection we study the influence of the positron wavefunction and e–p correlations on the calculated e–p momentum densities and positron lifetime. The contributions to $\rho(\boldsymbol{p})$, coming from valence and core electrons, are discussed separately. The e–p interaction is taken into account in the positron distribution through the e–p correlation potential, which is in turn associated with the e–p correlation function, γ, according to the Feynman theorem.

Both within the LDA and WDA, the energy dependent correlation functions have been incorporated in the calculation of partial and total annihilation rates according to (1) and (5) (the details of the approach are given in [9] and [10]). In the calculation of $\rho_{\mathrm{val}}(\boldsymbol{p} = \boldsymbol{k} + \boldsymbol{G})$, the energy factor $(E_{kj} - E_{01})/(\mu_- + E_{\mathrm{gap}} - E_{01})$ was employed in $\gamma(\boldsymbol{k}j, \boldsymbol{r})$ for the valence electron in the Bloch state $\boldsymbol{k}j$. In formula (5) for the total annihilation rate, the valence electron density was decomposed with respect to the angular momentum l and the corresponding centre-of-mass linearization energies [15, 16] were used instead of E_{kj} in the respective energy factor. For the core electrons, the relevant energy factor was set equal to zero in calculations of both the partial and total annihilation rates according to formulae (1) and (5). It should be pointed out that the semiconductor character of SiC is taken into account in the e–p correlation functions through the non-zero value of the energy gap, E_{gap}, in the energy factor defined above. In the calculation of the e–p momentum density and positron lifetime, a common approximation has been applied to the positron wavefunction and the e–p correlation functions, used in (1) and (5).

Finally, it should be mentioned here that the valence electrons give the main contribution to the e–p momentum density in the low momentum region, while the core electrons density dominates in the high momentum component (HMC) of $\rho(\boldsymbol{p})$. This effect is well observed in the experimental spectra, which correspond to the two- and one-dimensional projections of $\rho(\boldsymbol{p})$ and have been measured for SiC using the ACAR and two-detector coincidence Doppler techniques [4, 5], respectively.

2.3.1. Effect of the positron wavefunction. Let us concentrate on the influence of the positron wavefunction on the calculated e–p momentum density. Here a comparison of the EMD, which represents the uniform positron distribution (3), with the IPM e–p momentum density (2) provides a direct and unperturbed information on the overlap of the electron and positron wavefunctions. More specifically, the discrepancies between the EMD and IPM spectrum reflect just the sensitivity of the momentum densities in the material under study to the positron redistribution in the unit cell from the uniform distribution. On the other hand, past works have already established that the e–p correlation effects cannot be neglected in the calculation of the momentum density distribution for SiC [4]. For this reason we analyse the effect of the positron wavefunction on the calculated e–p momentum densities beyond the IPM as well. In the case of valence electrons in SiC, application of the LDA seems to be quite reliable, since these electrons show mainly s and p character with a small fraction of itinerant d electrons (cf figure 1). Consequently, in this subsection we study the valence contribution to the e–p momentum density calculated within the LDA to the e–p correlation functions in (1), $\gamma^{\mathrm{LDA}}(\boldsymbol{k}j, \boldsymbol{r})$ [9, 10, 13], incorporating various positron wavefunctions. For core electrons non-local e–p interaction effects start to play more important role, since the electron density is strongly varying close to the nuclei (cf figure 2) and therefore the non-local WDA seems to be more appropriate in this case than the LDA. For this reason we employ the WDA spectra, calculated according to (1) with $\gamma^{\mathrm{WDA}}(0, \boldsymbol{r})$ [10], in order to analyse the effect of positron wavefunction on the core electrons' contribution to the e–p momentum density.

The core part of the WDA e–p momentum density relative to EMD, $\rho_{\mathrm{core}}^{\mathrm{WDA}}(\boldsymbol{p})/\rho_{\mathrm{core}}^{\mathrm{EMD}}(\boldsymbol{p})$, calculated within various approximations to the positron wavefunction, is shown in the top panel of figure 5. Its IPM and EMD counterparts, $\rho_{\mathrm{core}}^{\mathrm{IPM}}(\boldsymbol{p})/\rho_{\mathrm{core}}^{\mathrm{EMD}}(\boldsymbol{p})$ and $\rho_{\mathrm{core}}^{\mathrm{EMD}}(\boldsymbol{p})$, are also presented. The relevant valence electrons contributions to the EMD, LDA and IPM e–p momentum density, $\rho_{\mathrm{val}}^{\mathrm{EMD}}(\boldsymbol{p})$, $\rho_{\mathrm{val}}^{\mathrm{LDA}}(\boldsymbol{p})$ and $\rho_{\mathrm{val}}^{\mathrm{IPM}}(\boldsymbol{p})$, are drawn in figure 6 for momenta $\boldsymbol{p}$ along [100] and [110] directions.

We shall start with the discussion of core electrons' contribution to ρ $(\boldsymbol{p})$. The first thing to note when comparing the IPM density, $\rho_{\mathrm{core}}^{\mathrm{IPM}}(\boldsymbol{p})$, with its EMD counterpart, $\rho_{\mathrm{core}}^{\mathrm{EMD}}(\boldsymbol{p})$, is that the core part of the resulting momentum density is significantly affected by the distortion of the positron density from the uniform distribution. The same effect is observed after including the e–p correlations to the formalism. The values of both the IPM and WDA e–p momentum densities are strongly reduced with respect to the EMD (at least five times in the low momentum region and over two orders of magnitude in the high momentum components).

The above features of the e–p momentum density are easy to explain. As can be seen in table 1 and figures 2 and 4, the major part of the positron density is accommodated in

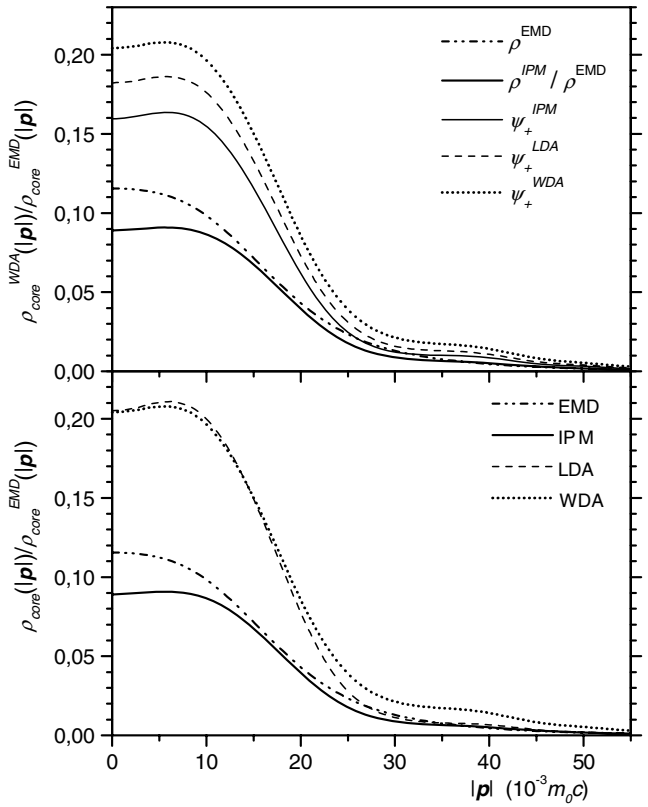

Figure 5. Momentum dependence of the calculated ratio of core e–p momentum densities to EMD, $\rho_{\rm core}(p)/\rho_{\rm core}^{\rm EMD}(p)$. The core electrons contribution to the EMD and relative IPM e–p momentum densities, $\rho_{\rm core}^{\rm EMD}(p)$ and $\rho_{\rm core}^{\rm IPM}(p)/\rho_{\rm core}^{\rm EMD}(p)$, are shown in both panels by the dash-dotted and bold solid lines, respectively. Top panel: the relative WDA spectra, $\rho_{\rm core}^{\rm WDA}(p)/\rho_{\rm core}^{\rm EMD}(p)$, obtained from (1) with $\gamma^{\rm WDA}(0,r)$ for $\psi_+^{\rm IPM}$, $\psi_+^{\rm LDA}$ and $\psi_+^{\rm WDA}$ (solid, dashed and dotted lines, respectively). Superscripts in ψ_+ refer to the approximation used for $V_{\rm corr}$ in (4*b*). EMD corresponds to the uniform positron distribution. Bottom panel: the relative spectra calculated within various approaches. The IPM, LDA and WDA (solid, dashed and dotted lines) denote the approximation applied to both the e–p correlation function, $\gamma(0,r)$, and the positron wavefunction, used in (1).

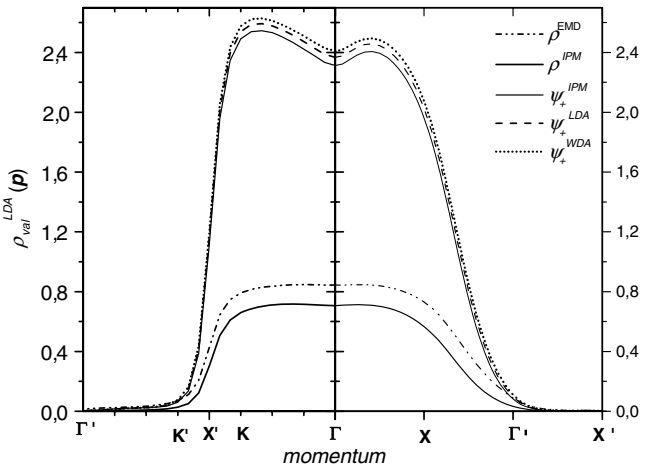

Figure 6. Valence electrons contribution to the electron–positron momentum density in SiC, $\rho_{\rm val}^{\rm LDA}(p)$, calculated within the LDA for $\psi_+^{\rm IPM}$, $\psi_+^{\rm LDA}$ and $\psi_+^{\rm WDA}$ (solid, dashed and dotted lines, respectively) used in (1), for momenta along [100] and [1101] directions. Superscripts in ψ_+ refer to the approximation used for $V_{\rm corr}$ in (4*b*). The EMD (3), which is due to the uniform positron distribution, $\rho_{\rm val}^{\rm EMD}(p)$, and the IPM e–p momentum density (2), $\rho_{\rm val}^{\rm IPM}(p)$, are shown by the dash-dotted and bold solid lines, respectively.

the interstitial region (empty spheres), while core electrons are localized just close to the centre of the Si and C spheres. In consequence, the overlap of the positron and electron wavefunctions in (1) and (2) is diminished appreciably as compared to the uniform positron distribution applied in (3). The behaviour of the IPM, LDA and WDA positron wavefunctions inside the spheres centred at the C and Si atoms has been analysed in details in section 2.2 and illustrated in the two upper panels of figure 4. The properties of $|\psi_+(\boldsymbol{r})|^2$ are well reproduced in the core part of the relevant WDA momentum densities, which are plotted in the top panel of figure 5. Once again, the conclusions, following from a comparison of the curves drawn in figure 5, are in agreement with the expectations. Taking into account the e–p interaction in the positron model (through the e–p correlation potential) increases the overlap of positron and core electron wave functions, as the positron surrounded by its screening cloud penetrates the ionic core region with higher probability than the 'bare' (IPM) particle. Here the non-locality of the e–p correlation potential enhances the above effect even further, as pointed out in the section 2.2. It is also apparent that the influence of the positron wavefunction on the resulting e–p momentum density is more pronounced in the low momentum region than in the HMCs.

As can be seen in figure 5, in the high momentum region (for momenta $p > 20$ mrad) the core part of EMD is not negligible. The high momentum component occurs in the calculated WDA e–p momentum density as well, although the positron redistribution in the Wigner–Seitz cell reduces the HMCs of $\rho_{\rm core}^{\rm WDA}(\boldsymbol{p})$ considerably as compared to EMD. Finally, it is worth to mention that the appearance of long tails in the e–p momentum density has been confirmed by the experiment, through the noticeable HMC, observed in the slope of coincidence Doppler broadening spectra measured for 3C SiC [4].

Let us now look in details at the valence part of the EMD, LDA and IPM e–p momentum densities, shown in figure 6 for the momenta along [100] and [110] directions. Comparing the curves plotted in figures 5 and 6, one can see that the influence of the positron wavefunction on the resulting momentum densities is qualitatively very similar for valence and core electrons. Once again, the positron localization in the interstitial region diminishes the values of the valence electrons contribution to the e–p momentum density noticeably, for the momenta both inside and outside the first Brillouin zone (BZ). This effect is well observed when comparing the IPM spectrum to its EMD counterpart. The reasons are similar as in the case of core electrons. However, in the first and second BZs the enhancement of the valence electrons density on the positron site, represented by the correlation functions $\gamma(\boldsymbol{k}j,\boldsymbol{r})$ in (1), suppresses the influence of the positron redistribution in the unit cell on the resulting e–p momentum density.

In consequence, for valence electrons the values of the LDA e–p momentum density are considerably greater than of its EMD counterpart, as can be seen in figure 6. Moreover, the valence part of the LDA (and IPM) e–p momentum density is quantitatively much less sensitive to the positron localization in the interstitial region and distribution in the unit cell than it is observed for core electrons, both in the low and high momentum region. In particular, in the high momentum region the effect of the positron wavefunction on the LDA e–p momentum density is not as significant for valence electrons as for core electrons. Neither in the low momentum region the influence of positron wavefunction is as pronounced in $\rho_{\rm val}^{\rm LDA}(\boldsymbol{p})$ as it occurs for core electrons. The above feature of $\rho_{\rm val}^{\rm LDA}(\boldsymbol{p})$ may be attributed to the fact that, in contrast to localized core electrons, the sp-type valence electrons in SiC are found in the empty spheres as well as close to the boundary of spheres centred at Si and C site, i.e. in the region in which the positron distribution has the highest weight. In consequence, the overlap of the positron and valence electron densities in the empty spheres does not vanish. Including the e–p correlation potential in the positron Schrödinger equation (4*b*) increases the values of $\rho_{\rm val}^{\rm LDA}(\boldsymbol{p})$ in the whole momentum space, especially for the momenta inside the first BZ. The non-locality of $V_{\rm corr}$ increases the e–p momentum density even further, as illustrated in figure 6. Once again, the choice of the positron model in (1) considerably less affects the resulting LDA e–p momentum density for valence than for core electrons.

2.3.2. Electron–positron correlation effect. Due to the strong Coulomb attraction between the positron and surrounding electrons, the electron density at the positron site, $\boldsymbol{r}$, is strongly enhanced from its initial value. This effect is described by the correlation functions, $\gamma(t, \boldsymbol{r})$, which in principle depend both on the initial electron state t and positron position $\boldsymbol{r}$. In turn, the positron interaction with the electron screening cloud gives rise to the e–p correlation potential, which affects the positron distribution. Both these effects should be included into the calculations of the positron annihilation characteristics within the common approach.

In this subsection the effect of the e–p interaction on the resulting momentum densities and total annihilation rates is discussed both within the LDA and WDA. In the bottom panel of figure 5 and in figure 7 we compare the EMD with the e–p momentum densities calculated within the IPM, LDA and WDA. The approach to the e–p interaction in (1) has been applied in the same way to both the e–p correlation functions and the positron wavefunction (through the e–p correlation potential).

It can be seen that the e–p interaction affects the e–p momentum densities considerably, both for core and valence electrons. Taking into account the e–p correlation functions leads to significant increase of the values of the resulting LDA and WDA spectra in the low momentum region, as compared to their IPM counterpart. For higher momenta, the negative slope of the core and valence momentum densities is observed. This effect is enhanced by inclusion of the e–p correlation functions. Outside the first BZ, the LDA and WDA curves are more quickly decreasing functions of momentum than the IPM

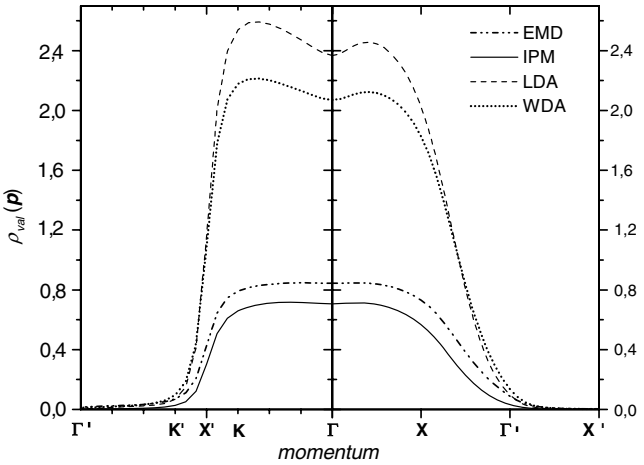

Figure 7. Electron–positron momentum densities in SiC calculated for valence electrons for momenta along [100] and [1101] directions. IPM, LDA and WDA (solid, dashed and dotted lines, respectively) refer to the approximation to both the e–p correlation function and positron wavefunctions incorporated in (1). The EMD (3) is shown by the dash-dotted line.

density. Here the position dependence of the e–p correlation functions, $\gamma(0, \boldsymbol{r})$ and $\gamma(\boldsymbol{k}j, \boldsymbol{r})$, plays the most important role, due to the strong variation of the relevant electron density, $n_{\rm el}(\boldsymbol{r})$.

For core electrons the influence of the positron redistribution in the unit cell dominates essentially over the effect of the enhancement of the electron density at the positron (described by the correlation functions $\gamma(0, \boldsymbol{r})$). The values of the LDA and WDA momentum densities do not exceed 25% of $\rho_{\rm core}^{\rm EMD}(\boldsymbol{p})$, as illustrated in the bottom panel of figure 5. In the low momentum region, the shape of the resulting core density is hardly sensitive to the non-locality of the e–p interaction. This is because the effect of non-locality in the positron wavefunction, which increases the values of $\rho_{\rm core}(\boldsymbol{p})$ with respect to LDA, is partially suppressed by the non-locality of correlation functions, $\gamma(0, \boldsymbol{r})$, which in turn diminishes the values of $\rho_{\rm core}(\boldsymbol{p})$. The latter property of WDA correlation functions may be attributed to shifting the weight of the electron screening cloud towards the region of high electron density, as mentioned in the preceding paragraphs. It can be also seen that in the high momentum region both the correlation functions and positron wavefunction, determined within the non-local WDA, enhance the HMC of core momentum density, while the HMC of the LDA spectrum is much more IPM-like. It should be remembered that the tails in the e–p momentum density correspond to the electron wavefunctions 'as seen' by a positron close to the nuclei. It is the region of high electron density in which the electron screening cloud, following from the non-local WDA approach, is strongly localized on the positron and the resulting enhancement of electron density on the positron site combined with a positron wavefunction, $\gamma^{\rm WDA}(0, \boldsymbol{r})|\psi_+^{\rm WDA}(\boldsymbol{r})|^2$, is much greater than its LDA counterpart, $\gamma^{\rm LDA}(0, \boldsymbol{r})|\psi_+^{\rm LDA}(\boldsymbol{r})|^2$.

Let us move back to valence electrons. As illustrated in figure 7 and mentioned in subsection 2.3.1, the effect of enhancement of the electron density on the positron position is

much stronger than the influence of the positron wavefunction on the calculated e–p momentum density, $\rho_{\rm val}(\boldsymbol{p})$, in both the low and high momentum regions. For the momenta inside the first BZ, values of the LDA and WDA momentum densities are noticeably greater than of their EMD counterpart. This is because the overlap of the positron and valence electrons wavefunctions is highest in the interstitial region, where the electron density is relatively low. The relevant values of correlation functions increase as compared to the core region, characterized by high electron density (the density dependence of correlation functions in an electron gas has been parameterized e.g. in [11]). Similarly as in the case of core electrons, the non-locality of the e–p interaction diminishes the values of $\rho_{\rm val}^{\rm WDA}(\boldsymbol{p})$ in the first BZ and increases them in the high momentum region, as compared to the LDA. However, this effect is quantitatively different for core and valence electrons.

For the momenta inside the first BZ, the shallow dips and valley can be seen close to the Γ point, both in the EMD and e–p momentum densities. Moreover, the LDA and WDA spectra show strong anisotropy. Both these effects are well observed in the experimental two-dimensional ACAR spectra [4]. Let us point out, that the dips in the EMD can be interpreted explicitly in terms of tetrahedral bonds in 3C SiC. Therefore, we can expect that the positron redistribution in the Wigner–Seitz cell should pronounce the behaviour of the spectra even further. However, incorporation of the positron wavefunction in (2) improves the agreement of theory with the experiment very slightly. As can be seen in figure 7, these are just the electron–positron correlation effects that provide considerable improvement of the agreement between the theory and experimental two-dimensional ACAR spectra [4]. Incorporating the energy dependent e–p correlation functions [9, 10] in (1) increases the anisotropy of $\rho_{\rm val}(\boldsymbol{p})$ in the first and second BZs. The humps and valley, seen in the spectra plotted in figure 7, are essentially enhanced in the LDA and WDA curves, especially for the momenta along the [110] direction. For the momenta along [100] direction the dip and bulge are shallower. This is just the result of energy dependence of the correlation functions, $\gamma(\boldsymbol{k}j, \boldsymbol{r})$. Due to the symmetry rules [21], for the momenta along [100] direction, only the first and second energy bands (shown in figure 1) contribute to the EMD and $\rho_{\rm val}(\boldsymbol{p})$, while for momenta along [110] direction there are first and third bands. Close to the BZ boundary, for momenta between $\boldsymbol{K}$ and $\boldsymbol{X}'$ points, the third band, which gives the main contribution to $\rho_{\rm val}(\boldsymbol{p} = \boldsymbol{k} + \boldsymbol{G})$, is strongly increasing function of energy. In consequence, the relevant correlation function, $\gamma(\boldsymbol{k}3, \boldsymbol{r})$, follows the momentum dependence of $E_{\boldsymbol{k}3}$. For the same reasons, for momenta between $\boldsymbol{X}'$ and $\boldsymbol{K}'$ points, the WDA and LDA curves show essentially more negative slope than their IPM and EMD counterparts. In contrast to the core electrons, the shape of the valence momentum density in the low momentum region and close to the first BZ boundary is visibly changed by the non-locality of the e–p interaction. Comparing the plots in figures 6 and 7 one can say, that the influence of non-locality in the correlation functions, $\gamma(\boldsymbol{k}j, \boldsymbol{r})$, on the resulting momentum density suppresses essentially the non-local effects, due to the positron wavefunction. For the momenta inside the first BZ and close to the BZ boundary, the WDA density has lower values and is a fairly less increasing function of momentum than its LDA counterpart. Concerning the slope of $\rho_{\rm val}^{\rm WDA}(\boldsymbol{p})$ close to the BZ boundary as compared to $\rho_{\rm val}^{\rm LDA}(\boldsymbol{p})$, this is the position dependence of the correlation functions, which leads to weaker momentum dependence of the WDA curve. The valence electrons density is polarized along the tetrahedral bonds and the weight of the screening charge distribution, obtained within the WDA, is localized there. This is also the reason why the effect of non-locality is more pronounced for the momenta along [110] direction and is weaker for the [100] direction.

In order to facilitate the verification of the present theory by experiment, in figure 8 we compare calculated and measured Doppler broadening spectra. The one-dimensional projections of the (spherically averaged) e–p momentum densities,

$$N(p_z) = C \int \rho(|\mathbf{p}|)\,\mathrm{d}p_x\,\mathrm{d}p_y = C2\pi \int_{|p_z|}^{\infty} p\rho(|\mathbf{p}|)\,\mathrm{d}p,$$

have been determined within the IPM, LDA and WDA. Constant C normalizes the positron annihilation probability density to the unit area. The theoretical spectra have been convoluted with the Gaussian, representing the experimental resolution function of [4]. Results are shown in the right panel of figure 8. The slope of the experimental Doppler broadening spectrum for 3C SiC has been retrieved from figure 1 of reference [4] by scan. In the left panel of figure 8 the experimental curve is presented together with the densities calculated in the reference [4] within the LDA. The core electrons contribution to the total (valence + core) momentum density is also quoted. As the total density has been normalized to the unit area, in consequence the area of the relevant core component is equal to the ratio of the core to total annihilation rates, $\lambda_{\rm core}/\lambda$ (cf formula (5)).

As can be seen in figure 8, in the high momentum region ($p_z > 20$ mrad) the main contribution to the total probability density comes from the core electrons, while the valence component dominates in $N(p_z)$ in the low momentum region. For both the valence and core electrons, the WDA results are intermediate between their LDA and IPM counterparts. For low momenta (up to 15 mrad), the WDA curve runs only a bit lower than the LDA plot. In this region the differences in the shape of the IPM, LDA and WDA probability densities, drawn in figure 8(b), are hardly seen. This indicates for very slight influence of the e–p correlations on the shape of the *isotropic* (spherically averaged) part of the valence electrons contribution to $N(p_z)$. A small bulge can be seen in the all three plots drawn in figure 8(b) as well as in the experimental spectrum shown in figure 8(a). This bulge, observed for momenta between 15 and 20 mrad, can be attributed to the oscillations in the HMCs of $\rho_{\rm val}(\boldsymbol{p})$. It can be seen in the valence EMD spectrum, presented in figure 6, that the Umklapp components of the electron wavefunctions, $\psi_{k1}(\boldsymbol{r})$, are not negligible for momenta $\boldsymbol{k}$ close to the $\boldsymbol{\Gamma}$ point (about 15% contribution). Although the positron redistribution strongly reduces the Umklapp components of the EMD in the

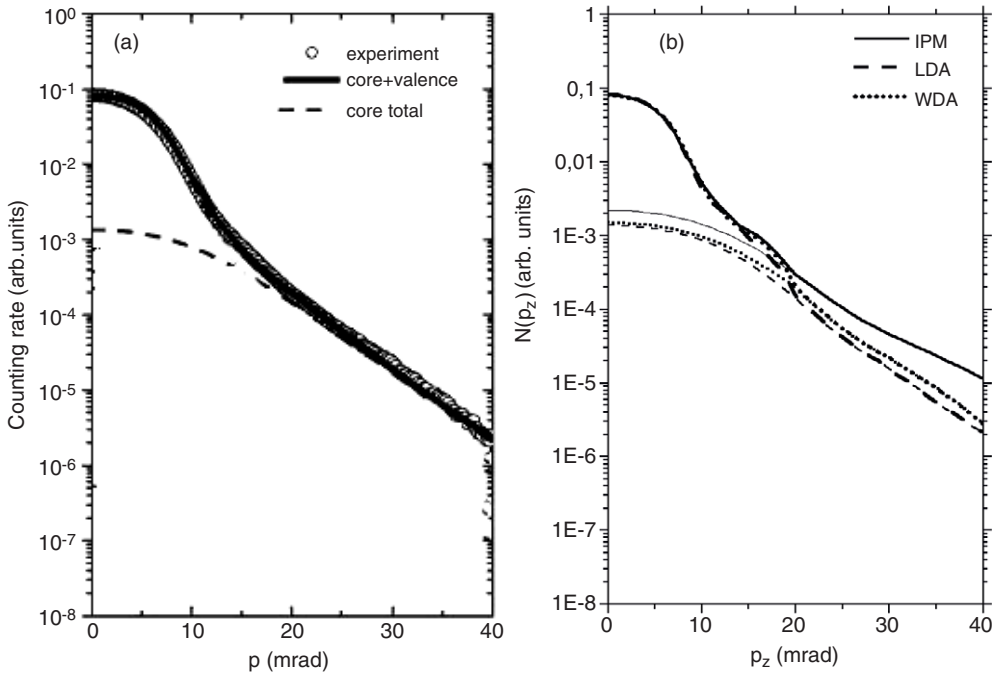

Figure 8. Theoretical one-dimensional projections of the total (valence + core) e–p momentum densities compared with experimental coincidence Doppler broadening spectra for 3C SiC. Spectra are normalized to the unit area. Theoretical densities are convoluted with the resolution function of the apparatus [4]. The contributions of the core electrons to the e–p momentum densities are also shown. Left panel: plots retrieved from figure 1 of reference [4]. Open circles refer to the experimental data. Solid and dashed lines represent the total and core probability density distributions, respectively, calculated in [4] within the LDA. Right panel: results of the present work obtained within the IPM, LDA and WDA approximations to the e–p correlations (solid, dashed and dotted lines). Bold and thin lines denote the total and core densities, respectively.

amplitudes of $\rho_{\rm val}(\boldsymbol{p} = \boldsymbol{k} + \boldsymbol{G})$, nevertheless the HMC of $\rho_{\rm val}(\boldsymbol{p} = \boldsymbol{k} + \boldsymbol{G})$ does not vanish close to the $\boldsymbol{\Gamma}''$ point. The situation changes for core electrons. The difference between the IPM, LDA and WDA densities is more pronounced in the core component of $N(p_z)$ than for the valence electrons. Moreover, the non-locality of the e–p correlation functions starts to play important role, as the electron charge density is strongly varying function close to the nuclei. For core electrons the WDA curve runs well above its LDA counterpart and in the high momentum region the WDA spectrum shows considerably larger tails.

The encouraging point is that the slopes of both the LDA and WDA probability densities, $N(p_z)$, agree with the experimental data reasonably well, with the accuracy of the thickness of circles, which mark the experimental data in figure 8(a). For low momenta (up to 15 mrad), both the LDA and WDA curves stick to the upper boundary of the experimental points. In the high momentum region (for $p_z > 20$ mrad), the experimental curve runs between the LDA and WDA results. The LDA and WDA spectra adhere, respectively, to the lower and upper boundary of circles representing the experimental data. It is worth to mention here that the slopes of the LDA spectrum, calculated in the present work and in reference [4], are quite similar, although present formalism bases on the state dependent correlation functions, in contrast to [4]. It should be also pointed out that the IPM spectrum differs from the LDA, WDA and experimental results appreciably, especially in the high momentum region.

Table 2. Positron lifetime (in ps) calculated within various approximations to the positron wavefunction and e–p correlation functions. Bold numbers refer to the common approach to both ψ_+ and γ. The reported experimental value amounts to 140 ps for perfect 6H SiC [2, 5, 6] and 142 ps for perfect 3C SiC [4].

	$\gamma^{\rm LDA}$	$\gamma^{\rm WDA}$
$\psi_+^{\rm IPM}$	141	157
$\psi_+^{\rm LDA}$	138	150
$\psi_+^{\rm WDA}$	132	144

Finally, let us compare the calculated and experimental values of the positron lifetime. Present results are listed in table 2. The experimental value amounts to 140 ps, measured for perfect 6H SiC [2, 5, 6] and 142 ps for perfect 3C SiC [4]. The theoretical values calculated in the present work (marked in bold in table 2) are equal to 138 and 144 ps for the LDA and WDA, respectively. Therefore, it is difficult to judge whether the LDA or WDA approach provides the better agreement with the experiment. Without a doubt, the IPM result of 480 ps is far unsatisfactory. Concerning the sensitivity of positron lifetime to the non-locality of the e–p correlations, the two effects compete with one another. As can be seen in table 2, the values of the positron lifetime, τ are diminished by the non-locality in the positron wavefunction (in the correlation potential $V_{\rm corr}$) and simultaneously increased by non-local effects in the correlation functions γ.

3. Conclusions

The aim of the present work is to study the influence of the positron distribution on the resulting annihilation characteristics. This effect has not been considered for SiC in any of references [2–8]. The next point is the sensitivity of the e–p momentum density to the non-local e–p correlation effects. It should be pointed out that although the authors of references [6, 7] thoroughly discuss the differences between the results obtained within the LDA and non-local GGA for the positron affinity and lifetime, nevertheless the e–p momentum densities have not been calculated in [6, 7].

In conclusion of present results, one could say that the momentum densities in SiC are very sensitive to the shape of the positron wavefunction in the Wigner–Seitz cell. In particular, the core part of $\rho(\boldsymbol{p})$ is significantly reduced with respect to its EMD counterpart. Taking into account the interaction of the positron with its screening cloud leads to a considerable redistribution of the positron wavefunction in the Wigner–Seitz cell. The weight of the positron density is shifted from the interstitial region towards the atomic cores, as the e–p correlation potential partially neutralizes the repulsive potential from the nuclei. This effect is enhanced within the non-local WDA approach. The influence of the shape of the positron wavefunction on the resulting e–p momentum densities for SiC is appreciable and it is due to the changes in the overlap of the positron and particular electron wavefunctions. This effect is pronounced in the low momentum region as well as in the HMCs of $\rho_{\mathrm{core}}(\boldsymbol{p})$.

Incorporating the electron–positron enhancement effects, through the correlation functions $\gamma(t, \boldsymbol{r})$, leads to significant improvement of the agreement between the resulting annihilation characteristics and experiment. The e–p interaction increases anisotropy of the valence contribution to the e–p momentum density, $\rho_{\mathrm{val}}(\boldsymbol{p})$, as compared to the IPM result. Non-locality of the e–p interaction changes the values of $\rho(\boldsymbol{p})$ and $N(p_z)$ in the low momentum region rather slightly, for both valence and core electrons. In contrast to the low momentum region, the HMC of the core spectrum is very sensitive to this non-locality.

All the above properties of the e–p momentum densities are exactly reproduced, both quantitatively and qualitatively, in the core and valence components of the total annihilation rate, λ, and hence in the positron lifetime, $\tau = 1/\lambda$. The incorporation of the e–p interaction leads to the essential improvement of the agreement between the theory and experiment. Concerning the non-locality of the e–p correlations, the experimental positron lifetime [2, 4, 5] and Doppler broadening spectra [4] are intermediate between the LDA and WDA results.

References

[1] For review and references see e.g. Puska M J and Nieminen R M 1994 *Rev. Mod. Phys.* **66** 841
Nieminen R M 1996 *Positron Spectroscopy of Solids* ed A Dupasquier and A P Mills (Amsterdam: IOS Press) p 443
Berko S 1983 *Positron Solid State Physics* ed W Brandt and A Dupasquier (Amsterdam: North-Holland) p 64
Nieminen R M 1983 *Positron Solid State Physics* ed W Brandt and A Dupasquier (Amsterdam: North-Holland) p 105

[2] Choyke J, Marsumari H and Persl G (ed) 2004 *Silicon Carbide—Recent Major Advances* (Berlin: Springer) For review and references see e.g. http://www.ioffe.rssi.ru/SVA/NSM/Semicond/SiC/bandstr.html

[3] Ayma D, Lichanot A and Rerat M 1999 *J. Phys. Chem.* B **103** 5441
Ayma D, Rerat M, Orlando R and Lichanot A 1998 *Acta Crystallogr.* A **54** 1019 (part 6, Sp. Iss. 2)

[4] Kawasuso A, Yoshikawa M, Itoh H, Chiba T, Higuchi T, Betsuyaku T, Redmann F and Krause-Rehberg R 2005 *Phys. Rev.* B **72** 045204

[5] Kawasuso A, Chiba T and Higuchi T 2005 *Phys. Rev.* B **71** 193204

[6] Kuriplach J, Sob M, Brauer G, Anward W, Nicht E M, Coleman P G and Wagner N 1999 *Phys. Rev.* B **59** 19489
Brauer G, Anwand W, Nicht E M, Kuriplach J, Sob M, Wagner N, Coleman P G, Puska M J and Konhonen T 1996 *Phys. Rev.* B **54** 2512
Panda B K, Brauer G and Skorupa Wand Kuriplach J 2000 *Phys. Rev.* B **61** 15848

[7] Kuriplach J, Sob M, Puska M J, Brauer G, Anward W, Nicht E M, Coleman P G and Wagner N 1996 *Abstr. Pap. Am. Chem. Soc.* **211** 74 Nucl Part 2
Kuriplach J, Brauer G, Anwand W and Skorupa W 2003 *Phys. Rev. Lett.* **91** 199601

[8] Rubaszek A 2006 *Proc. 36th Seminar on Positron Annihilation (Turawa, 2006)*; *Acta Phys. Pol.* A **110** 683

[9] Daniuk S, Sob M and Rubaszek A 1991 *Phys. Rev.* B **43** 2580

[10] Rubaszek A, Szotek Z and Temmerman W M 1998 *Phys. Rev.* B **58** 11285
Rubaszek A, Szotek Z and Temmerman W M 2000 *Phys. Rev.* B **61** 10100

[11] Nieminen R M and Puska M J 1983 *Phys. Rev. Lett.* **50** 281
Boronski E and Nieminen R M 1986 *Phys. Rev.* B **34** 3820

[12] Barbiellini B, Puska M J, Konhonen S T, Hajru A and Nieminen R M 1996 *Phys. Rev.* **53** 1620

[13] Sormann H and Kontrym-Sznajd G 2006 *Phys. Rev.* B **73** 075111
Kontrym-Sznajd G, Samsel-Czekala M, Pietraszko A and Sormann H 2002 *Phys. Rev.* B **66** 155110

[14] Gunnarson O, Johnson M and Lundqvist B I 1979 *Phys. Rev.* B **20** 3136
Jensen K O and Walker A B 1988 *J. Phys. F: Met. Phys.* **18** 1277

[15] Andersen O K 1975 *Phys. Rev.* B **12** 3600
Lambrecht W R L and Andersen O K 1986 *Phys. Rev.* B **34** 2439

[16] Skriver H L 1984 *The LMTO Method. Muffin-Tin Orbitals and Electronic Structure* ed M Cardona and P Fulde (Berlin: Springer)

[17] Jarlborg T and Singh A K 1987 *Phys. Rev.* B **36** 4660

[18] Ceperley D M and Alder B J 1980 *Phys. Rev. Lett.* **45** 566
Perdew J P and Zunger A 1981 *Phys. Rev.* B **23** 5048

[19] Perdew J P and Wang Y 1986 *Phys. Rev.* B **35** 8800
Burke D 1988 *Phys. Rev.* A **38** 3098
Perdew J P and Wang Y 1992 *Phys. Rev.* B **45** 13244

[20] Puska M J, Lanki P and Nieminen R M 1989 *J. Phys.: Condens. Matter* **1** 6081

[21] Harthoorn P and Mijnarends P E 1978 *J. Phys. F: Met. Phys.* **8** 1147